ACS NANO Cite This: ACS Nano XXXX, XXX, XXX–XXX www.acsnano.org

ARTICLE

Twists and Turns of Orbiting and Spinning Metallic Microparticles Powered by Megahertz Ultrasound

Chao Zhou,† Leilei Zhao,† Mengshi Wei, and Wei Wang*

Harbin Institute of Technology (Shenzhen), Shenzhen, Guangdong 518055, China

Supporting Information

ABSTRACT: Micromotors powered by megahertz ultrasound, first reported about 5 years ago, have lately been considered a promising platform for a wide range of microscale applications, yet we are only at the early stage of understanding their operating mechanisms. Through carefully designed experiments, and by comparing the results to acoustic theories, we present here an in-depth study of the behaviors of particles activated by ultrasound, especially their in-plane orbiting and spinning dynamics. Experiments suggest that metallic microrods orbit in tight circles near the resonance ultrasound frequency, likely driven by localized acoustic streaming due to slightly bent particle shapes. On the other hand, particle spins around their long axes on nodal lines, where phase-mismatched orthogonal sound waves possibly produce a viscous torque. Intriguingly, such a torque spins metal-dielectric Janus microspheres back and forth in an unusual "rocking chair" fashion. Overall, our observations and analysis provide fresh and much needed insights on the interesting particle dynamics in resonating ultrasound and could help with developing more powerful and controllable micromachines with biocompatible energy sources.

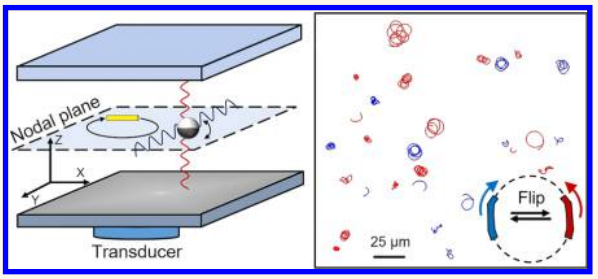

KEYWORDS: *micromotors, nanomotors, mechanisms, ultrasound manipulation, external fields, biocompatible, Janus*

Micromachines, especially those that move autonomously at colloidal or nanometer scales, have always captured popular imagination.[1−4] In recent years, laboratory implementations of micromachines have emerged; some inspired by living animals and micro-organisms[5−8] and others driven by a slew of chemical,[9−11] electromagnetic,[12−15] thermal,[16] and optical effects[17−21] that in one way or another breaks symmetry and generates gradients.[22] One of the latest development is the use of megahertz ultrasonic standing waves to power the motion of metallic microparticles.[23,24] When suspended in water and levitated by ultrasonic standing waves, metallic microrods exhibit three distinctive types of fast dynamics (Figure 1 and Video S1): in-plane directional motion (Figure 1a), in-plane orbiting in tight circles (Figure 1b), and spinning about their long axes (Figure 1c).[23] However, the advancement in this field is still limited by our relatively poor understanding of their individual operating mechanisms, as well as their spatial inhomogeneity: groups of metallic rods at different locations on the nodal plane can exhibit different types of motion in Figure 1, with seemingly little pattern to follow (see, for example, supporting videos of ref 23).

Given the mounting popularity of micromotor research, the ultrasound powered directional motion (Figure 1a) has received the largest share of attention among the three modes of motion.[24] For example, preliminary but exciting applications of these "acoustic micromotors" have been

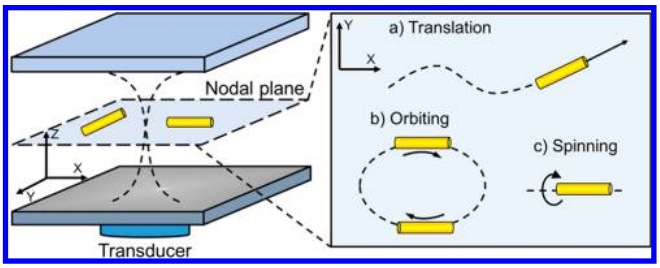

Figure 1. Schematics of three distinct modes of motion for metal microrods in ultrasonic standing waves (Video S1). Particles levitate to a central nodal plane and exhibit in-plane directional motion (a), orbiting (b), and spinning (c). Particle and device sizes are not to actual scale.

reported in the field of nanomedicine.[25−28] Although a few possible mechanisms for such directional motion were proposed,[23,28] the one based on near-particle acoustic streaming is quickly gaining popularity.[29,30] The orbiting and spinning motion of metal rods in ultrasound (Figure 1b,c), on the other hand, are equally interesting but much less understood. These two modes of motion might prove quite useful in micro-

Received: October 10, 2017
Accepted: November 28, 2017
Published: November 28, 2017

DOI: 10.1021/acsnano.7b07183
ACS Nano XXXX, XXX, XXX–XXX

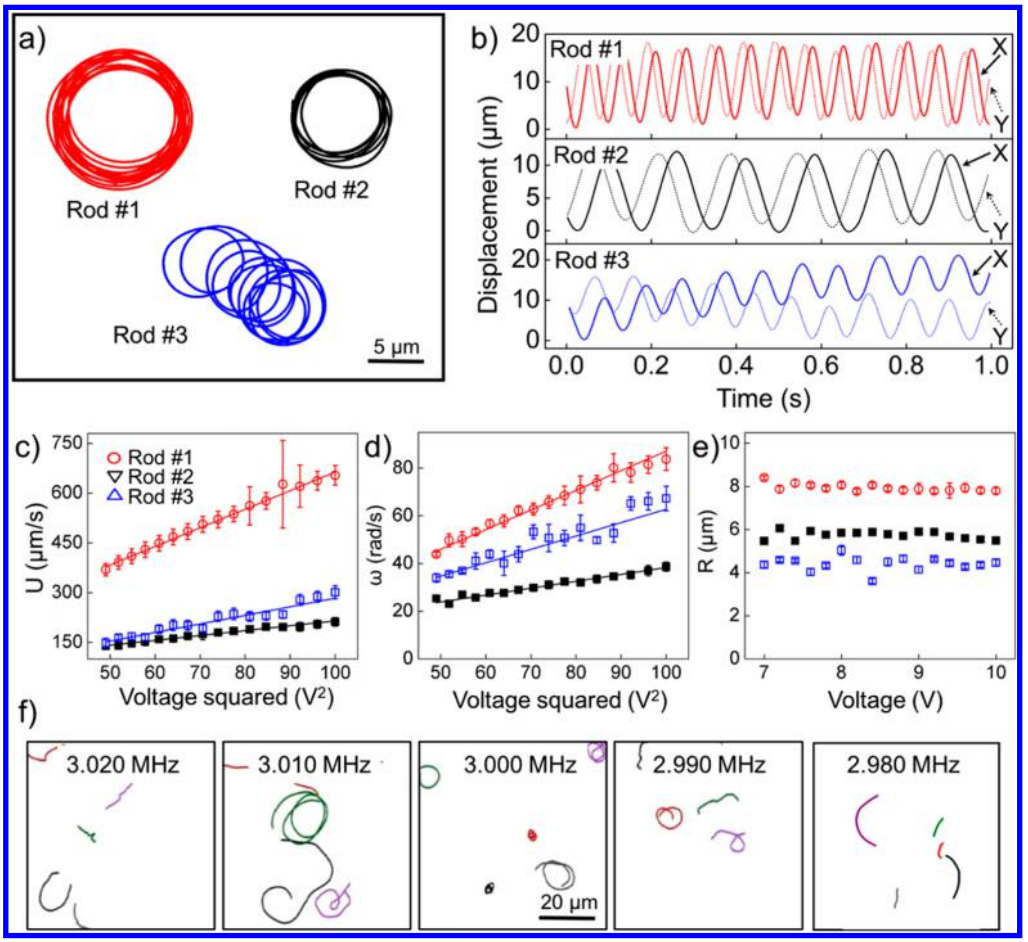

Figure 2. Single particle dynamics of three microstirrers. (a) Trajectories of three orbiting rods on the levitation plane during 1.0 s. These rods moved at different speeds, possibly because of their differences in the degree of shape asymmetry. (b) Displacement of the same three rods along *X* (solid) and *Y* (dashed) directions. (c–e) As voltage increases, the linear speeds *U* (c) and angular speeds ω (d) of microstirrers scale to V^2, while their orbiting radii *R* (e) remain nearly constant. Solid lines are linear fits. (f) As the ultrasound frequency shifts away from the resonance frequency (3.000 MHz in this case), the trajectories of orbiting rods change from circles to more linear and random shapes.

machinery, such as microdrillers[31,32] or microstirrers,[33−35] and can serve as biocompatible alternatives to more commonly studied chemical or electromagnetic counterparts. A better understanding of the ultrasound powered rotating and spinning of microparticles, however, is required for applications beyond proof-of-concepts.

To this end, we combined carefully analyzed experiments with recent acoustic theories to advance our understanding of the orbiting and spinning motion of metallic (and half-metallic) microparticles powered by MHz ultrasonic standing waves. Their orbiting and chirality-flipping dynamics suggest that streaming-induced in-plane torques operating at single particle levels are likely responsible for their rotation. On the other hand, the spinning dynamics of SiO_2−Ti Janus microspheres could be semiquantitatively accounted for by streaming-induced viscous torques due to phase-mismatched incident sound waves propagating in different directions. Finally, a tentative but unified picture is given to explain how and when the three modes of ultrasound powered motion in Figure 1 occur, a topic that has haunted researchers in this field since the very beginning. This study therefore provides insight in the general interaction between sound and matter, at the same time advancing our capability in designing more powerful and controllable micromachines powered by ultrasound.

RESULTS AND DISCUSSION

Our ultrasound experiments were carried out in a homemade setup (see Methods and Figure S1 in Supporting Information that is available online). A nodal plane at the center of the chamber forms at the resonance ultrasound frequency, where particles move by Figure 1; this plane is where all the following experiments were conducted. In a typical experiment, a chamber height of ∼200 μm and a resonance frequency of ∼3 MHz was used. Ultrasound propagates in the *Z* direction, and a nodal plane forms in the *XY* direction at half the height of the chamber. To prevent possible confusion, we note that particles in ultrasound do NOT simultaneously orbit in tight circles (Figure 1b) and spin along their long axes (Figure 1c). Spinning rods sometimes assemble into long chains along which they shuttle (Video S1, right panel). Although these chains can curve into wide circles (see Figure 3c and 3e in ref 23), they are quite different from the tight circles discussed here. Spinning spheres, either completely metal or Janus, in general do not undergo translational motion but only assemble into chains or cluster unless they are of asymmetric shapes.

Orbiting Motion of Individual Metallic Microrods in Ultrasound. We first focus on the in-plane orbiting motion of metallic microrods (hereafter referred to as "microstirrers") in ultrasound (Figure 1b). These microrods of 300 nm in diameter and ∼2 μm in length were synthesized by electro-

DOI: 10.1021/acsnano.7b07183
ACS Nano XXXX, XXX, XXX−XXX

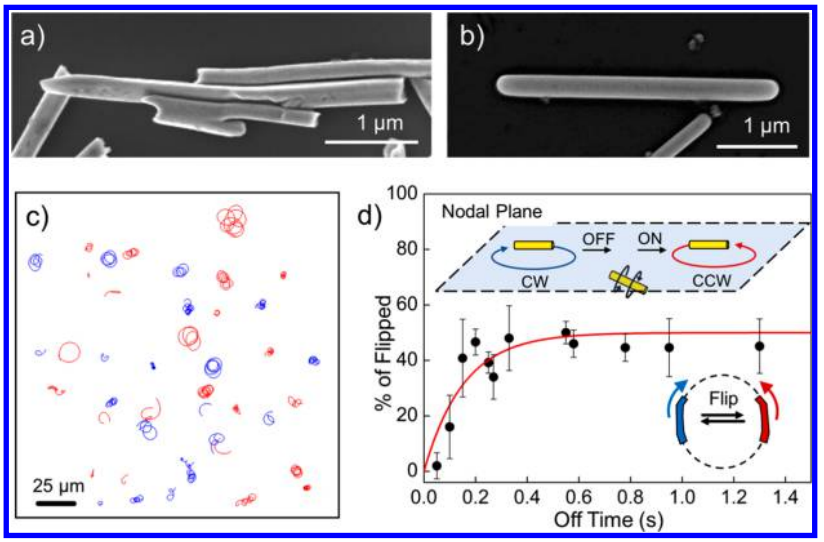

Figure 3. On the orbiting mechanism of metal microrods. (a,b) Scanning electron micrographs of gold microrods (a) with noticeable shape imperfections, and a silver microrod (b) of almost perfectly cylindrical shape. (c) Optical micrograph showing gold microrods orbiting on the nodal plane either clockwise (CW, blue) or counterclockwise (CCW, red), taken from Video S5. Particle trajectories are overlaid for 0.67 s (80 frames). (d) Sketch of how rods reverse their chirality after power interruptions, and the reversal ratio as a function of ultrasound off time. Solid line: fitting by $y = 0.5-0.5[1 - \exp(-x/\tau_c)]$. The fitting result for the characteristic flipping time τ_c of a rod is 0.154 s. Inset on bottom right: cartoon illustrating that a bent rod could rotate CW or CCW depending on how its body is placed on the plane, which is completely random. Rotation in CW and CCW directions is therefore equally probable. This cartoon is for illustrating the concept only, and we do not conclusively know whether a rod rotates toward the bent side.

depositing gold in porous alumina membranes (see Methods section for details). However, rods made of platinum, ruthenium, and rhodium would all show qualitatively the same orbiting dynamics as well as directional motion[36] since the acoustic contrast factor of these metals (including silver), which determines the magnitude of the acoustic radiation force they experience, is very similar. Near the resonance frequency, microrods moved in tight and independent circles, and Figure 2a shows the smoothed trajectories of three of such rods moving at different locations on the XY plane. Their angular velocity, ω, can be extracted from the periodic oscillation of their coordinates in X or Y (Figure 2b), while their linear speeds U were calculated from their displacement between each subsequent frame (120 frames per second). The radius R of their circular trajectories follows $R = U/\omega$, assuming perfect circles, although imperfect circular trajectories were also common (see Figure 3c and Video S5 for examples).

A number of experimental parameters significantly affect the orbiting dynamics (*i.e.*, R, U, and ω) of microstirrers. In a recent study, Ahmed *et al.* have reported an increase in orbiting radii for rods located farther away from lateral nodes.[36] Here, we focus on the effect of the driving voltage V and frequency f on the orbiting dynamics of microstirrers (results shown in Figure 2). The speed U of an orbiting rod (and its angular velocity ω) scales to V^2, consistent with the results for the translational motion of acoustic micromotors.[36] Video S2 shows rods moving at three different voltages. Such a dependency has previously been explained by an acoustic streaming theory,[29,30] where acoustic motor's lateral speed on the nodal plane scales to the second order of the displacement amplitude a in the vertical direction, which is further proportional to the driving voltage V (*i.e.*, $U \sim a^2 \sim V^2$).

Ultrasound frequency is another important parameter governing the dynamics of microparticles; a slight shift in the driving frequency can significantly undermine the capability of rods to orbit in circles. Instead, their trajectories became more random and less close-looped, and their linear speeds decreased (Video S3). This is captured in Figure 2f where the trajectories of a few moving rods are shown at five different frequencies around the resonance frequency (3.000 MHz). Such a sharp transition from circular orbits to open and more linear trajectories could be due to the sensitivity of the acoustic resonator to the driving frequency of a high Q transducer, combined with the inability of nonresonant ultrasound to prevent rods from flipping around their bodies by Brownian rotation. Both of these factors will be discussed in more details in a later section.

Why do metal rods orbit in ultrasound? It is easy to imagine the electrodeposited microrods might not be perfectly cylindrical; alumina templates might contain defects within their pores or not be perfectly straight. An electron micrograph of a few of such imperfect gold microrods is presented in Figure 3a as an example. It has been recently proposed that the front and end shape asymmetry of a metallic microrod leads to asymmetric surface acoustic streaming, which propels the particle into directional motion.[29,30] Similarly, a rod containing protrusions or cavities on its side, or more likely is slightly curved, could experience an uneven distribution of forces and torques on the nodal plane and therefore rotate in-plane. To test this hypothesis, control experiments were performed with silver microrods of similar dimension to the gold rods used above, but of almost perfect shape symmetry (Figure 3b; see Methods for synthesis details). When suspended in ultrasound standing waves, they levitate and align (Video S4) but never showed directional propulsion or orbiting, lending strong support to the acoustic streaming mechanism involving shape asymmetry.

Group of Independent Microstirrers. Following the acoustic streaming theory and its dependency on particle shape asymmetry at a single particle level, one naturally wonders if this can be verified within a larger population via ensemble statistics. One way is to examine the spatial-temporal

DOI: 10.1021/acsnano.7b07183
ACS Nano XXXX, XXX, XXX−XXX

distribution of the rotation chirality, that is, rotation in clockwise (CW) or counterclockwise (CCW), of a group of microstirrers. For example, we have determined the chirality of a group of microstirrers in Video S5 to be ~50% CW and ~50% CCW (Figure 3c, color coded), and such a ratio is stable during our observation time. In addition, we note that any individual rod that is levitated would spin in constant chirality, rather than switching between CW and CCW from time to time. This is an important feature of orbiting rods that will be discussed in more details later.

It is also interesting to examine how the ensemble chirality ratio might change from its steady state 50−50% when the system is disrupted and, in doing so, whether the chirality reverses for any particular rod. The reasoning is that a consistent chirality at both a single particle and an ensemble level despite interruptions might indicate the presence of a time-invariant local energy distribution which is responsible for rod orbiting (*e.g.*, some sort of local flow or acoustic torque that is independent of how the rod is placed). To test this, pulsed ultrasound was applied with varying time periods in which the power was off ("off time"; see Supporting Information for details), as opposed to the continuous ultrasound that was used for all the other experiments. Upon turning off the ultrasound, microstirrers immediately became inactive (except for Brownian motion) and began to sediment slightly but quickly returned to their orbiting motion when the ultrasound was resumed. The off time was tuned from 0.05 to 1.3 s, beyond which accurate particle tracking was difficult because of sedimentation. We confirm that every time the system recovered from power interruption, ~50% of rods consistently orbited in CW and the other ~50% in CCW, that is, interruption at the probed time scale did not change the ensemble chirality distribution. At a single particle level, however, some rods switched their individual chirality after power interruptions (*i.e.*, from CW to CCW or *vice versa*), and the percentage of these switched rods (referred to as "flipping" hereafter) increased from ~0% at off time of 0.05 s to ~50% at off time of ~0.4 s and beyond (Figure 3d). It naturally follows that, to maintain an ensemble 50−50% chirality ratio, roughly equal number of rods switched from CW to CCW and from CCW to CW. Both are counted to acquire the flipping statistics.

The above ensemble results are reasonable if the imperfectness of rods are considered and suggest that the orbiting motion is likely due to torques generated at a single particle level. To elaborate, since there was no preferred 2D orientation for a freely suspended rod, it (along with its imperfect features shown in Figure 3a) could face "right" or "left" (when seen from the top) on the levitation plane, and thus could rotate in CW or CCW at equal probabilities (see Figure 3d inset). Although the orientation was mostly fixed for an orbiting microstirrer (discussed later), after the sound was turned off, it was allowed to rotate randomly along both axes while sedimenting. Its imperfect features therefore randomly spun. Note that this spinning of rods during sedimentation is due to thermal fluctuation, rather than being powered by ultrasound, and is therefore fundamentally different from the spinning motion in Figure 1c and that discussed in later sections. This purely thermal fluctuation yielded a spinning rate about the long axis of ~7 Hz, which corresponded to a characteristic spinning time τ_c of ~0.144 s for a typical rod (2 μm long, 300 nm in diameter; see Supporting Information for calculation details).[37,38] As a result, half of all rods were expected to flip their orientation if they were allowed to sediment for an off time much longer than τ_c and therefore reversed their chirality when ultrasound was resumed. The probability for a rod to flip decays exponentially at shorter off times when a rod does not have enough time to rotate its body. This is exactly what we observed, and the measured reversal ratio at different off time in Figure 3d can be fit by a Boltzmann function with a τ_c of 0.154 s, which agrees reasonably well with our calculated value of 0.144 s. The above analysis further supports the hypothesis that rods orbit due to their shape asymmetry.

Before we move on to the next section on particle spinning, we would like to comment on the interesting observation that an *orbiting* microstirrer does NOT spontaneously change its chirality, even though theories predict that it would randomly reorient (and thus reverse its chirality) ~7 times a second, regardless of where and how it rotates. To understand this apparent inconsistency, we hypothesize that the orientation of acoustic microstirrers in action is somehow confined and flipping would require overcoming a large energy barrier, unless when ultrasound is stopped or weakened. Such a hypothesis echoes that proposed by Takagi *et al.*, where curved bimetallic microrods having sizes and shapes very similar to those studied here, but operating by a completely different phoretic mechanism, tend to move along twisted trajectories and circular paths.[37] They argue that the close proximity to bottom walls of these chemical micromotors creates an energy barrier that hinders their otherwise random flipping, which, unlike for perfect cylinders, requires a substantial amount of energy for an asymmetric cylinder. Although physical boundaries are absent in our experiments, acoustic radiation force traps a levitated rod on the nodal plane, with an energy barrier that could prove too high for a trapped rod to flip. This is also consistent with a previously described observation that, as the ultrasound frequency was moved away from the resonance frequency, rods started to move in less circular trajectories (Figure 2f), presumably because the acoustic force in this case was too weak to confine their orientations.

Spinning of Metal-Coated Janus Microspheres in Ultrasound. Besides directional and orbiting motion, metallic rods also spin about their long axes in ultrasound (Figure 1c). This is most striking when a large cluster of metallic microrods spin collectively (Video S6); their vortex hydrodynamically couples to each other and forms a large spindle that dynamically reconfigures its shape and size. In a previous study, Balk *et al.* carefully monitored the convective motion of small polystyrene tracers near a spinning gold rod in ultrasound.[39] By extrapolation, they determined that the rod spun as fast as 2.5 kHz. However, to understand the spinning mechanism, it is critical to directly visualize and study the spinning of a particle. To this end, metallic microrods are no longer useful because it is impossible to tell how a microrod spins with the resolution offered by a regular optical microscope. Instead, Janus microspheres (*i.e.*, of two chemically or physically different hemispheres) were used in the current study. Although Janus spheres could spin differently from metallic microrods due to their differences in particle geometry and compositions, the knowledge acquired from the current investigation could shed light on a general understanding of how particles spin in ultrasound. These Janus spheres were prepared by evaporating a thin layer (20 nm) of metal titanium (Ti) on top of a monolayer of silicon dioxide (SiO_2) beads (5 μm in diameter). The Ti and SiO_2 hemisphere appears dark and bright under a bright-field microscope, respectively, thus

DOI: 10.1021/acsnano.7b07183
ACS Nano XXXX, XXX, XXX−XXX

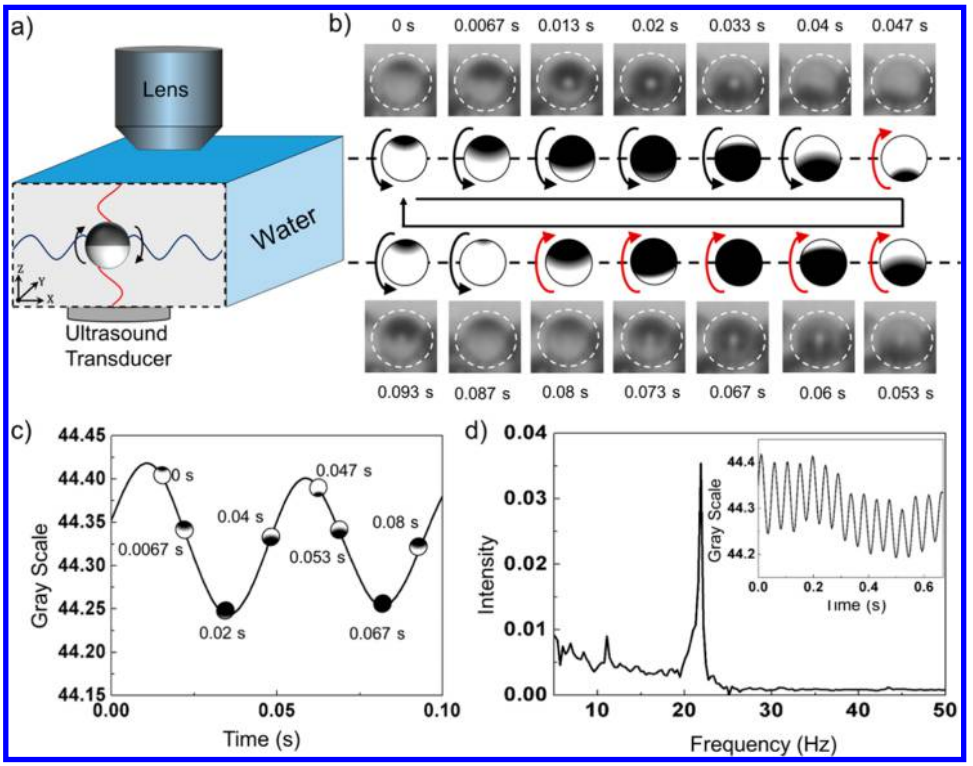

Figure 4. Spinning dynamics of an individual SiO_2−Ti Janus microsphere in ultrasound. (a) Sketch of the experimental setup and a cross section, highlighting the torques acting on a sphere due to the phase-mismatched ultrasound waves traveling in *X* and *Z* directions. (b) Time series snapshots and cartoon illustrations of the "moon phases" of a spinning SiO_2−Ti Janus microsphere of 5 μm in diameter. The black and red arrows indicate opposite spinning directions. Since SiO_2 is not transparent enough to see the material covered underneath, the particle appears "white" whenever the metal layer is flipped behind the focal plane. This is also helpful in identifying the transition from ~0.04 to 0.05 s as flipping backward, rather than spinning in the original direction. (c) Average gray value of the circled area in (b) as a function of time, with particle orientations overlaid. (d) Power spectra by fast Fourier transform of a representative spinning sphere. The major peak at ~20 Hz corresponds to the particle spinning frequency.

providing sufficient optical contrast for the easy identification of the particle orientation and calculation of its spinning rate.

When levitated in ultrasound, these SiO_2−Ti Janus microspheres could remain individual but more often are grouped into chains or clusters, possibly due to secondary radiation forces (*i.e.*, Bjerknes forces) that are attractive in-plane.[40] Like the metal rods that spin about their long axes, these Janus beads also spun, with their metal and silica hemispheres flipping in and out of focus in turns (Figure 4a and Video S7). Because of the difference in optical contrast between the two hemispheres, a spinning Janus particles demonstrated "moon phases" that are captured in Figure 4b. However, we particularly note that they do NOT rotate the full 360° but rather back and forth in a "rocking chair" fashion, which will be discussed in more details later.

The spinning dynamics of a Janus microsphere can be characterized by following the changes in its optical contrast (Figure 4). For example, a series of optical micrographs of a spinning Janus microsphere are captured at different time steps (Figure 4b), showing various moon phases. Next, this Janus sphere was isolated by computer codes from its neighbors. The average gray values of every pixel on this Janus bead was then examined over time (Figure 4c), and a periodic change was recorded. Fast Fourier transform (FFT) was then performed on this series of oscillating gray values (Figure 4d), and the highest intensity in the power spectrum corresponds to the spinning frequency of the sphere.

Unfortunately, such a method of isolating and analyzing individual particles becomes impractical when large clusters are concerned, where reliable single particle tracking is difficult. Instead, an ensemble analysis was used (illustrated in Figure 5) to provide the statistics of spinning frequency of Janus particles in a cluster. The general procedure is as follows. First, the gray value of *one pixel* in a given frame was recorded over time (Figure 5b), and its fluctuation was converted to a power spectrum by FFT (Figure 5c). This process was then repeated for all other pixels in the frame, and their spectra in the frequency domain were combined (Figure 5d). Finally, a weighted average was performed on the filtered signals by multiplying each frequency with its corresponding intensity (probability), yielding the average spinning rates of the cluster. This is then plotted against ultrasound frequency (Figure 5e) and voltage (Figure 5f), showing a trend similar to that of an individual microsphere (data not shown). In addition, the frequency dependency in Figure 5e can be fit by a mechanical resonator model (see Supporting Information for details),[41] suggesting that our acoustic chamber operates with a resonance frequency of 4.02 MHz and a quality factor (Q) of 29.5. This is consistent with the experimentally observed resonance frequency, and with the fact that ultrasound propulsion significantly weakened as the frequency was moved away from resonance. Furthermore, this suggests the possibility to use spinning Janus microparticles as a simple tool to characterize *in situ* the resonance properties of acoustic devices.

DOI: 10.1021/acsnano.7b07183
ACS Nano XXXX, XXX, XXX−XXX

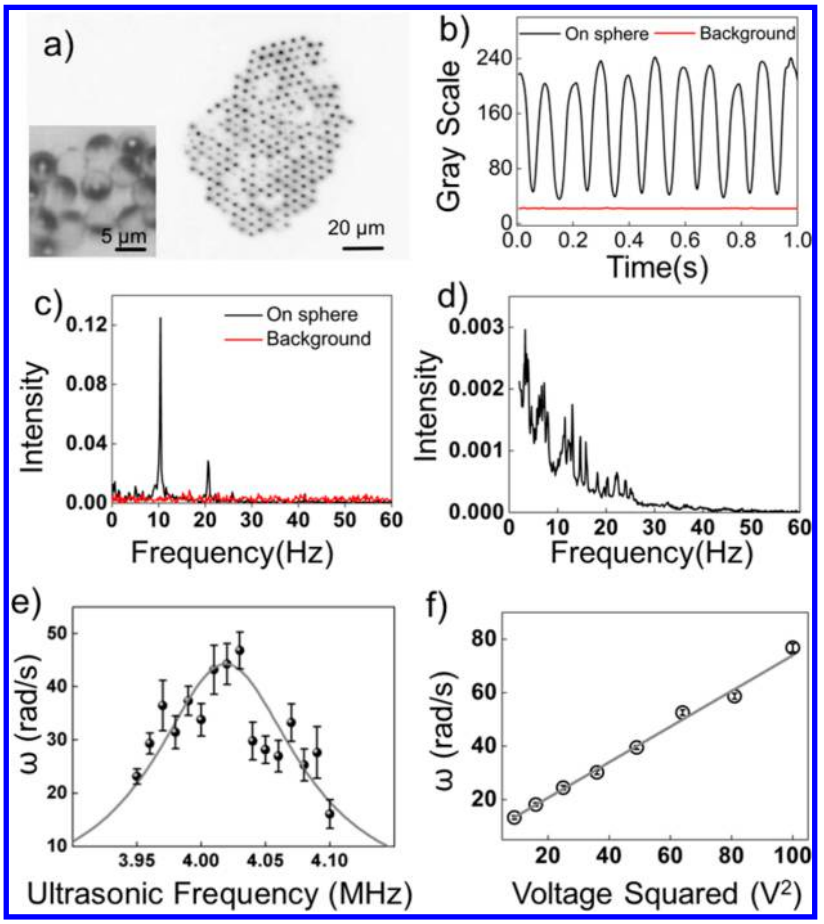

Figure 5. Analysis of spinning microspheres in a cluster. (a) Optical micrograph of a cluster of SiO_2−Ti Janus microspheres of 5 μm in diameter (inset: a magnified picture showing moon phases). (b) Time evolution of the gray values of two pixels, one on a spinning sphere and the other on the background. (c) Fast Fourier transform of (b). (d) Combined power spectra of all pixels in (a). The presence of multiple peaks indicates that Janus spheres in the same cluster spin at different rates. (e) Average spinning rate of spheres in a cluster at different driving frequencies and a Lorentz fit (see Supporting Information for fitting details). (f) Average spinning rate of spheres in a cluster scales to the second power of the driving voltage.

Spinning Mechanisms. Following the local acoustic streaming due to particle shape asymmetry, which have been used in previous sections to explain the translational and rotational in-plane motion of metallic microrods in ultrasound, one might naturally suspect that spinning discussed in this section is also due to the same shape asymmetry effect. However, even perfectly symmetric particles such as polystyrene or silica microspheres and silver microrods (Figure 3b) would spin (in different magnitude) on the nodal plane, similar to Janus microspheres described here. Such an insensitivity to shape and materials suggests that the spinning mechanism has little to do with shape-induced local streaming but, we propose, much to do with the way sound waves propagate in the experimental chamber. To elaborate, although in our experiments the transducer operates in the thickness mode and sound waves primarily travel along the Z direction (and therefore forms a nodal plane on the XY plane; see Figure S1 for an illustration of the experiment setup), wave propagation on the XY plane was also found. This is a common feature for thickness mode ultrasound chambers and possibly due to sound scattering from their side walls.[42−44] As a result, a particle in our experiments could experience sound waves propagating in X, Y, and Z directions, all with the same wavelengths but likely of different phases.

Importantly, it is known that such orthogonal standing waves shifted in phase could induce surface acoustic streaming and generate torques on even axisymmetric particles.[45−47] If we, for the sake of simplicity, only consider the streaming-induced torque $\Gamma^{\text{streaming}}$ generated by the sound waves in the X and Z directions, then[46]

$$\Gamma^{\text{streaming}} = \frac{3\pi r_0^2 \delta_\eta}{\rho_0 c_0^2} p_{0x} p_{0z} \sin(\varphi) \tag{1}$$

where r_0 is the particle radius, ρ_0 is the density of medium (water), c_0 is the sound speed in the medium, p_{0x} and p_{0z} are the acoustic pressure amplitude along the X and Z directions, respectively, φ is the phase difference between waves in X and Z directions, and δ_η is the viscous penetration depth, which is further given by

$$\delta_\eta = \sqrt{\frac{2\eta}{\rho_0 f}} \tag{2}$$

where η is the fluid viscosity and f is the driving frequency of the ultrasound. This torque at low Reynolds number is balanced by the viscous torque:[46]

$$\Gamma_\eta = 8\pi\eta r_0^3 \omega \tag{3}$$

DOI: 10.1021/acsnano.7b07183
ACS Nano XXXX, XXX, XXX−XXX

where ω is the spinning rate of a particle. By balancing the two torques in eqs 1 and 3, we obtain the spinning rate

$$\omega = \sqrt{\frac{18}{64\rho_0^3 f\eta}}\, p_{0x}p_{0z}\sin(\varphi)/r_0c_0^2 \quad (4)$$

Following eq 4, we can therefore estimate of the spinning rate of a 5 μm Janus sphere in our experiments, provided the following assumptions. First, the phase lag φ is assumed to be exactly $\pi/2$, which would yield the largest torque and fastest spin. Second, we assume that the sound wave traveling in the X direction is 1 order of magnitude weaker than that in the Z (major) direction (*i.e.*, $p_{0x} = 0.1p_{0z}$). This is considered reasonable because the side walls in our acoustic chamber are made of silicone, which is significantly softer and of lower acoustic contrast than the rigid top and bottoms (glass and silicon wafer, respectively). Finally, a typical value of 1 bar (10^5 Pa) is used for the pressure amplitude in the Z direction p_{0z}, which is a common value reported in the literature for similar acoustic setups.[45] Following these assumptions, we calculated a spin rate of 47.7 rad/s that is very close to experimentally measured value (~45 rad/s at the resonance frequency; see Figure 5e). This close match is certainly very sensitive to the above assumptions but nevertheless supports to some extent the validity of eq 4 and the viscous torque hypothesis responsible for particle spinning.

Before we finish our discussion on the spinning mechanisms of Janus spheres, we note that this mechanism predicts a full 360° spin, while the SiO_2−Ti Janus particles only spun partially (*i.e.*, a back and forth "rocking chair" motion). Our own experiments with other dielectric-metal spheres and various experimental cells showed similar results. On the contrary, a previous study by Lamprecht *et al.* found that PMMA−gold Janus spheres rotated full circles under orthogonal sound waves from two transducers on the XY plane.[45] Other than their different transducer configuration, we note that the diameters of the spheres used in their study (71−650 μm) were significantly larger than the one used in the current study (a few micrometers), while the metal coating thickness is similar (~20 nm). Therefore, the acoustic response of their samples and ours could be different, which could explain the observed difference in spinning dynamics but also indicates the complexity of this fundamental question.

CONCLUSION

To summarize, we have performed an in-depth experimental study on two distinct modes of rotational motion of microparticles powered by megahertz ultrasound: orbiting in a tight circle and spinning about their long axes. At the acoustic resonance frequency, metal microrods orbit both clockwise and counterclockwise in equal probabilities, with an angular frequency that scales to the second power of the driving voltage. They were able to flip their chirality if allowed to sediment for longer than a characteristic rotational diffusion time, suggesting that the asymmetric features at a single particle level are responsible for their orbiting motion. Microparticles in ultrasound also spin in and out of the nodal plane, and this was studied carefully with SiO_2−Ti Janus microspheres. Surprisingly, these spheres do not spin in full circles but only back and forth similar to a rocking chair. Their spin rates also scale to the second power of the driving voltage, and the frequency dependency matches that of a mechanical resonator with a quality factor of 29.5. Such a spontaneous spinning could be due to the interactions of sound waves traveling along multiple axes, all in the same frequency but at different phases. The resulting viscous torque from surface acoustic streaming induces particle spinning.

Overall, our study, in conjunction with previous studies,[23,29,30,36] proposes a consistent and unified picture of how megahertz ultrasonic standing wave power microparticles into three modes of motion *via* surface streaming. Specifically, when particles are located where sound waves from different directions interact, possible spinning (Figure 1c) due to viscous torques entails. Otherwise, they could be powered elsewhere into orbiting in tight circles (Figure 1b) when resonance frequency was applied or into more random and linear trajectories (Figure 1a) if the frequency is slightly off-resonance. Particle shape asymmetry, either at the tips or the sides, plays a critical role in the generation of asymmetric streaming and therefore powered motion/rotation, consistent with theoretical predictions. Unsolved mysteries still linger, but our greatly improved understanding of ultrasound powered micromotors, stirrers, and spinners could prove useful in designing more efficient and versatile micromachines.

METHODS

Sample Synthesis and Fabrication. Gold microrods were synthesized by electrodeposition in alumina templates following a procedure adapted from an earlier study.[48] Porous AAO membranes (Whatman) with a nominal pore diameter of 200 nm were used. Before electrodeposition, 200−300 nm of silver was thermally evaporated on one side of the membrane as the working electrode. The membrane was then assembled into an electrochemical cell with the pore openings immersed in the metal plating solution. Silver plating solution (Alfa Aesar) and homemade gold solution (gold content 28.7 g/L) were used. In a typical experiment, 5−10 μm of silver was first electrodeposited into the pores at −5 mA/cm^2, followed by gold at −0.2 mA/cm^2, the length of which can be controlled by monitoring the charges passed. The silver segment and the membrane were then dissolved in HNO_3 and NaOH solution, respectively, and gold rods were released and cleaned in DI water. Silver microrod samples were provided by Prof. Yejun Qiu and were synthesized following a classic technique published previously.[49]

Ultrasound Experiment. A typical ultrasound experiment cell (see Figure S1) is assembled by a silicon wafer, a PZT ceramic transducer (Steminc, part no. SMD12T06R412WL, resonance frequency 3.4 MHz), and a silicone spacer of 250 μm in height with a hole of 5 mm in diameter (Grace Biolabs). A piece of silicon wafer was used as the substrate, and the ceramic disk was fixed to its rough back by epoxy and connected to a waveform generator (Keysight 33510B). On the front (smooth) side of the wafer sits the silicone spacer, with a glass coverslip on the top. Particle suspension was then loaded into the chamber by micropipet, and ultrasound frequency was tuned to achieve half-wavelength standing waves (*i.e.*, resonance frequency). A few layers of Kapton tape, or rectangular glass capillary tubes (Vitrocom, part no. 3520), can also be used as the experimental chamber, provided that proper height was obtained. Pulsing ultrasound was applied by setting up the waveform generator in burst mode (see Supporting Information for details). Experiments were conducted on an Olympus BX51 M upright microscope, and videos were recorded with a CMOS camera (Point Gray, model Grasshopper 3). Particle coordinates were tracked by homebrew MATLAB codes courtesy of Hepeng Zhang from SHJT University.

ASSOCIATED CONTENT

Supporting Information

The Supporting Information is available free of charge on the ACS Publications website at DOI: 10.1021/acsnano.7b07183.

DOI: 10.1021/acsnano.7b07183
ACS Nano XXXX, XXX, XXX−XXX

Brief description of the ultrasound experiment setup, calculation of the rod flipping frequency, description of fitting the mechanical resonator, and descriptions of the seven video files (PDF)
Video S1 (AVI)
Video S2 (AVI)
Video S3 (AVI)
Video S4 (AVI)
Video S5 (AVI)
Video S6 (AVI)
Video S7 (AVI)

AUTHOR INFORMATION

Corresponding Author

*E-mail: weiwangsz@hit.edu.cn or wwang.hitsz@gmail.com.

ORCID

Wei Wang: 0000-0003-4163-3173

Author Contributions

†C.Z. and L.Z. contributed equally.

Notes

The authors declare no competing financial interest.

ACKNOWLEDGMENTS

W.W. is grateful for the helpful discussions with Profs. T. Mallouk, J. Sader, H.P. Zhang, J. Gibbs, N. Wu, and Dr. H. Kandula, and for the silver microrod samples provided by Prof. Y. Qiu at HIT-Shenzhen. This work is financially supported by National Science Foundation of China (11402069 and 11774075), Natural Science Foundation of Guangdong Province (No. 2107B030306005), Science Technology and Innovation Program of Shenzhen (JCYJ20170307150031119), and Harbin Institute of Technology.

REFERENCES

(1) Whitesides, G. M. The Once and Future Nanomachine. *Sci. Am.* **2001**, *285*, 78−83.
(2) Ozin, G. A.; Manners, I.; Fournier-Bidoz, S.; Arsenault, A. Dream Nanomachines. *Adv. Mater.* **2005**, *17*, 3011−3018.
(3) Mallouk, T. E.; Sen, A. Powering Nanorobots. *Sci. Am.* **2009**, *300*, 72−77.
(4) Wang, J. *Nanomachines: Fundamentals and Applications*; John Wiley & Sons: Hoboken, NJ, 2013.
(5) Magdanz, V.; Sanchez, S.; Schmidt, O. G. Development of A Sperm-Flagella Driven Micro-Bio-Robot. *Adv. Mater.* **2013**, *25*, 6581−6588.
(6) Ahmed, D.; Baasch, T.; Jang, B.; Pane, S.; Dual, J. r.; Nelson, B. J. Artificial Swimmers Propelled by Acoustically Activated Flagella. *Nano Lett.* **2016**, *16*, 4968−4974.
(7) Palagi, S.; Mark, A. G.; Reigh, S. Y.; Melde, K.; Qiu, T.; Zeng, H.; Parmeggiani, C.; Martella, D.; Sanchez-Castillo, A.; Kapernaum, N.; et al. Structured Light Enables Biomimetic Swimming and Versatile Locomotion of Photoresponsive Soft Microrobots. *Nat. Mater.* **2016**, *15*, 647−653.
(8) Dreyfus, R.; Baudry, J.; Roper, M. L.; Fermigier, M.; Stone, H. A.; Bibette, J. Microscopic Artificial Swimmers. *Nature* **2005**, *437*, 862−865.
(9) Sánchez, S.; Soler, L.; Katuri, J. Chemically Powered Micro-and Nanomotors. *Angew. Chem., Int. Ed.* **2015**, *54*, 1414−1444.
(10) Dey, K. K.; Sen, A. Chemically Propelled Molecules and Machines. *J. Am. Chem. Soc.* **2017**, *139*, 7666−7676.
(11) Moo, J. G. S.; Mayorga-Martinez, C. C.; Wang, H.; Khezri, B.; Teo, W. Z.; Pumera, M. Nano/Microrobots Meet Electrochemistry. *Adv. Funct. Mater.* **2017**, *27*, 1604759.
(12) Chen, X.-Z.; Hoop, M.; Mushtaq, F.; Siringil, E.; Hu, C.; Nelson, B. J.; Pané, S. Recent Developments in Magnetically Driven Micro-and Nanorobots. *Appl. Mater. Today* **2017**, *9*, 37−48.
(13) Xu, T.; Gao, W.; Xu, L. P.; Zhang, X.; Wang, S. Fuel-Free Synthetic Micro-/Nanomachines. *Adv. Mater.* **2017**, *29*, 1603250.
(14) Fischer, P.; Ghosh, A. Magnetically Actuated Propulsion at Low Reynolds Numbers: Towards Nanoscale Control. *Nanoscale* **2011**, *3*, 557−563.
(15) Kim, K.; Guo, J.; Xu, X. B.; Fan, D. L. Recent Progress on Man-Made Inorganic Nanomachines. *Small* **2015**, *11*, 4037−4057.
(16) Lin, X.; Si, T.; Wu, Z.; He, Q. Self-Thermophoretic Motion of Controlled Assembled Micro-/Nanomotors. *Phys. Chem. Chem. Phys.* **2017**, *19*, 23606−23613.
(17) Xu, L.; Mou, F.; Gong, H.; Luo, M.; Guan, J. Light-Driven Micro/Nanomotors: From Fundamentals to Applications. *Chem. Soc. Rev.* **2017**, *46*, 6905−6926.
(18) Dong, R.; Hu, Y.; Wu, Y.; Gao, W.; Ren, B.; Wang, Q.; Cai, Y. Visible-Light-Driven Bioi-Based Janus Micromotor in Pure Water. *J. Am. Chem. Soc.* **2017**, *139*, 1722−1725.
(19) Dai, B.; Wang, J.; Xiong, Z.; Zhan, X.; Dai, W.; Li, C.-C.; Feng, S.-P.; Tang, J. Programmable Artificial Phototactic Microswimmer. *Nat. Nanotechnol.* **2016**, *11*, 1087−1092.
(20) Palacci, J.; Sacanna, S.; Steinberg, A. P.; Pine, D. J.; Chaikin, P. M. Living Crystals of Light-Activated Colloidal Surfers. *Science* **2013**, *339*, 936−940.
(21) Zhou, D.; Ren, L.; Li, Y. C.; Xu, P.; Gao, Y.; Zhang, G.; Wang, W.; Mallouk, T. E.; Li, L. Visible Light-Driven, Magnetically Steerable Gold/Iron Oxide Nanomotors. *Chem. Commun.* **2017**, *53*, 11465−11468.
(22) Wang, W.; Duan, W.; Ahmed, S.; Mallouk, T. E.; Sen, A. Small Power: Autonomous Nano-and Micromotors Propelled by Self-Generated Gradients. *Nano Today* **2013**, *8*, 531−554.
(23) Wang, W.; Castro, L. A.; Hoyos, M.; Mallouk, T. E. Autonomous Motion of Metallic Microrods Propelled by Ultrasound. *ACS Nano* **2012**, *6*, 6122−6132.
(24) Rao, K. J.; Li, F.; Meng, L.; Zheng, H.; Cai, F.; Wang, W. A Force to Be Reckoned With: A Review of Synthetic Microswimmers Powered by Ultrasound. *Small* **2015**, *11*, 2836−2846.
(25) Wu, Z.; Li, T.; Li, J.; Gao, W.; Xu, T.; Christianson, C.; Gao, W.; Galarnyk, M.; He, Q.; Zhang, L.; et al. Turning Erythrocytes into Functional Micromotors. *ACS Nano* **2014**, *8*, 12041−12048.
(26) Wang, W.; Li, S.; Mair, L.; Ahmed, S.; Huang, T. J.; Mallouk, T. E. Acoustic Propulsion of Nanorod Motors inside Living Cells. *Angew. Chem., Int. Ed.* **2014**, *53*, 3201−3204.
(27) Garcia-Gradilla, V.; Sattayasamitsathit, S.; Soto, F.; Kuralay, F.; Yardımcı, C.; Wiitala, D.; Galarnyk, M.; Wang, J. Ultrasound-Propelled Nanoporous Gold Wire for Efficient Drug Loading and Release. *Small* **2014**, *10*, 4154−4159.
(28) Garcia-Gradilla, V.; Orozco, J.; Sattayasamitsathit, S.; Soto, F.; Kuralay, F.; Pourazary, A.; Katzenberg, A.; Gao, W.; Shen, Y.; Wang, J. Functionalized Ultrasound-Propelled Magnetically Guided Nanomotors: Toward Practical Biomedical Applications. *ACS Nano* **2013**, *7*, 9232−9240.
(29) Nadal, F.; Lauga, E. Asymmetric Steady Streaming as a Mechanism for Acoustic Propulsion of Rigid Bodies. *Phys. Fluids* **2014**, *26*, 082001.
(30) Collis, J. F.; Chakraborty, D.; Sader, J. E. Autonomous Propulsion of Nanorods Trapped in an Acoustic Field. *J. Fluid Mech.* **2017**, *825*, 29−48.
(31) Gibbs, J.; Fischer, P. Active Colloidal Microdrills. *Chem. Commun.* **2015**, *51*, 4192−4195.
(32) Xi, W.; Solovev, A. A.; Ananth, A. N.; Gracias, D. H.; Sanchez, S.; Schmidt, O. G. Rolled-up Magnetic Microdrillers: Towards Remotely Controlled Minimally Invasive Surgery. *Nanoscale* **2013**, *5*, 1294−1297.
(33) Guzmán-Lastra, F.; Kaiser, A.; Löwen, H. Fission and Fusion Scenarios for Magnetic Microswimmer Clusters. *Nat. Commun.* **2016**, *7*, 13519.

DOI: 10.1021/acsnano.7b07183
ACS Nano XXXX, XXX, XXX−XXX

(34) Kim, K.; Xu, X.; Guo, J.; Fan, D. Ultrahigh-Speed Rotating Nanoelectromechanical System Devices Assembled from Nanoscale Building Blocks. *Nat. Commun.* **2014**, *5*, 3632.
(35) Kim, K.; Guo, J.; Liang, Z. X.; Zhu, F. Q.; Fan, D. L. Man-Made Rotary Nanomotors: A Review of Recent Developments. *Nanoscale* **2016**, *8*, 10471−10490.
(36) Ahmed, S.; Wang, W.; Bai, L.; Gentekos, D. T.; Hoyos, M.; Mallouk, T. E. Density and Shape Effects in the Acoustic Propulsion of Bimetallic Nanorod Motors. *ACS Nano* **2016**, *10*, 4763−4769.
(37) Takagi, D.; Braunschweig, A. B.; Zhang, J.; Shelley, M. J. Dispersion of Self-Propelled Rods Undergoing Fluctuation-Driven Flips. *Phys. Rev. Lett.* **2013**, *110*, 038301.
(38) Ortega, A.; Garcıa de la Torre, J. Hydrodynamic Properties of Rodlike and Disklike Particles in Dilute Solution. *J. Chem. Phys.* **2003**, *119*, 9914−9919.
(39) Balk, A. L.; Mair, L. O.; Mathai, P. P.; Patrone, P. N.; Wang, W.; Ahmed, S.; Mallouk, T. E.; Liddle, J. A.; Stavis, S. M. Kilohertz Rotation of Nanorods Propelled by Ultrasound, Traced by Microvortex Advection of Nanoparticles. *ACS Nano* **2014**, *8*, 8300−8309.
(40) Gröschl, M. Ultrasonic Separation of Suspended Particles-Part I: Fundamentals. *Acta Acust. Acust.* **1998**, *84*, 432−447.
(41) Sader, J. E.; Yousefi, M.; Friend, J. R. Uncertainty in Least-Squares Fits to the Thermal Noise Spectra of Nanomechanical Resonators with Applications to the Atomic Force Microscope. *Rev. Sci. Instrum.* **2014**, *85*, 025104.
(42) Barmatz, M.; Collas, P. Acoustic Radiation Potential on a Sphere in Plane, Cylindrical, and Spherical Standing Wave Fields. *J. Acoust. Soc. Am.* **1985**, *77*, 928−945.
(43) Kaduchak, G.; Sinha, D. N.; Lizon, D. C. Novel Cylindrical, Air-Coupled Acoustic Levitation/Concentration Devices. *Rev. Sci. Instrum.* **2002**, *73*, 1332−1336.
(44) Raeymaekers, B.; Pantea, C.; Sinha, D. N. Manipulation of Diamond Nanoparticles Using Bulk Acoustic Waves. *J. Appl. Phys.* **2011**, *109*, 014317.
(45) Lamprecht, A.; Schwarz, T.; Wang, J.; Dual, J. Viscous Torque on Spherical Micro Particles in Two Orthogonal Acoustic Standing Wave Fields. *J. Acoust. Soc. Am.* **2015**, *138*, 23−32.
(46) Bernard, I.; Doinikov, A. A.; Marmottant, P.; Rabaud, D.; Poulain, C.; Thibault, P. Controlled Rotation and Translation of Spherical Particles or Living Cells by Surface Acoustic Waves. *Lab Chip* **2017**, *17*, 2470−2480.
(47) Schwarz, T.; Petit-Pierre, G.; Dual, J. Rotation of Non-Spherical Micro-Particles by Amplitude Modulation of Superimposed Orthogonal Ultrasonic Modes. *J. Acoust. Soc. Am.* **2013**, *133*, 1260−1268.
(48) Wang, Y.; Hernandez, R. M.; Bartlett, D. J.; Bingham, J. M.; Kline, T. R.; Sen, A.; Mallouk, T. E. Bipolar Electrochemical Mechanism for the Propulsion of Catalytic Nanomotors in Hydrogen Peroxide Solutions. *Langmuir* **2006**, *22*, 10451−10456.
(49) Sun, Y.; Yin, Y.; Mayers, B. T.; Herricks, T.; Xia, Y. Uniform Silver Nanowires Synthesis by Reducing $AgNO_3$ with Ethylene Glycol in the Presence of Seeds and Poly(Vinyl Pyrrolidone). *Chem. Mater.* **2002**, *14*, 4736−4745.

DOI: 10.1021/acsnano.7b07183
ACS Nano XXXX, XXX, XXX−XXX